Electronic Supplementary Information

Isoindigo-Based Low Bandgap Conjugated Polymer for *o*-Xylene Processed Efficient Polymer Solar Cells with Thick Active Layers

Xin Dong,[ab] Yunfeng Deng,[a] Hongkun Tian,*[a] Zhiyuan Xie,[a] Yanhou Geng,*[a] Fosong Wang [a]

[a]*State Key Laboratory of Polymer Physics and Chemistry, Changchun Institute of Applied Chemistry, Chinese Academy of Sciences Changchun, 130022, P. R. China.*

[b]*University of Chinese Academy of Sciences, Beijing, 100049, P. R. China*

Corresponding author: yhgeng@ciac.ac.cn; hktian@ciac.ac.cn

Instruments: ^{1}H and ^{13}C NMR spectra were recorded on a Bruker AV 400 MHz spectrophotometer with chloroform-d ($CDCl_3$) as solvent and tetramethylsilane (TMS) as an internal standard. High-temperature gel permeation chromatography (GPC) was performed by using 1,2,4-trichlorobenzene as eluent and polystyrene as standard at 150 ^{o}C on a PL-GPC 220 system. UV-Vis absorption spectra were measured on a Shimadzu UV3600 UV-vis-NIR spectrometer. Cyclic voltammetry (CV) measurements were carried out on a CHI660a electrochemical workstation using saturated calomel electrode (SEC) as reference electrode, platinum wire as counter electrode and glassy carbon electrode (diameter of 1 cm) as working electrode. TGA was carried out at a heating rate of 10 °C/min under nitrogen flow on a PerkinElmer TGA7. DSC was performed on a PerkinElmer DSC 7 with a heating/cooling rate of ±10 °C/min under nitrogen flow. Atomic force microscopy (AFM) measurements were carried out in tapping mode on a SPA400HV instrument with a SPI 3800 controller (Seiko Instruments). Transmission electron microscopy (TEM) images were recorded on a JEM-1011 transmission electron microscope with accelerating voltage of 100 KV and camera length of 160 cm. Thin film XRD were tested on Bruker D8 Discover X- ray diffractometer (out-plane) and Rigaku SmartLab X- ray diffractometer (in-plane) with an incidence angle of 0.2°, Cu Kα as X-ray sourse (λ = 0.154 nm), tube voltage of 40 KV and electric current of 200 mA. Two dimensional grazing incidence X-ray diffraction (GIXD) was measured at Shanghai Synchrotron Radiation Facility (SSRF) on beam line BL14B1 (λ = 0.124 nm) with a MarCCD area detector at incidence angle of 0.16^{o}.

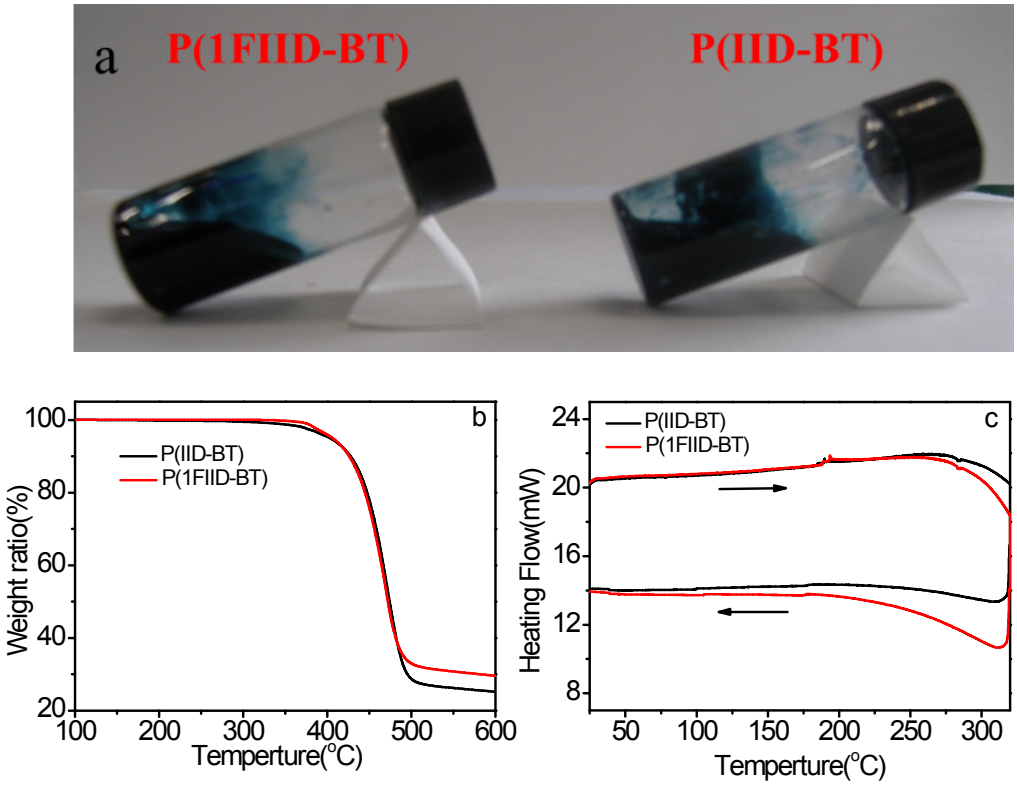

Fig. S1 (a): Photos of the solutions of P(1FIID-BT) and P(IID-BT) (5 mg/mL) in *o*-xylene prepared at 80 °C after stored at room temperature for 3 hours. P(1FIID-BT) solution was stable while P(IID-BT) began to precipitate. TGA (b) and DSC (c) curves of P(1FIID-BT) and P(IID-BT).

Table S1. Molecular Weight and Solubility of P(1FIID-BT) and P(IID-BT).

polymer	M_n [kDa]	M_W [kDa]	Đ	*o*-DCB[a]	*o*-xylene[a]
P(IID-BT)	25	82	3.24	S	P
P(1FIID-BT)	65	219	3.36	S	S

[a] The concentrations of P(1FIID-BT) and P(IID-BT) were 12 mg/mL in *o*-DCB and 5 mg/mL in *o*-xylene. P: precipitation; S: solution.

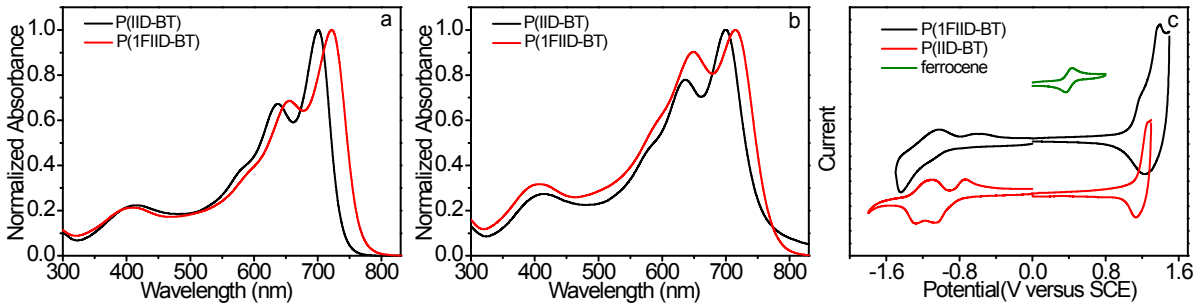

Fig. S2 Solution (a) (1.0×10^{-5} mol/mL in *o*-xylene for P(1FIID-BT) and *o*-DCB for P(IID-BT)) and film (b) absorption spectra and film cyclic voltammograms (c) of P(1FIID-BT) and P(IID-BT).

Table S2. Optical and Electrochemical Properties of Polymers

polymer	UV-vis λ_{max}[nm]		E_g^{opt} [eV]	Cyclic voltammetry			
	Solution	Film		E_{onset}^{ox}[a] [eV]	E_{onset}^{re}[a] [eV]	HOMO [eV]	LUMO [eV]
P(IID-BT)	420/639/701	420/638/701	1.65	0.64	-1.28	-5.44	-3.52
P(1FIID-BT)	412/658/722	410/650/716	1.61	0.66	-1.23	-5.46	-3.57

[a] The oxidation and reduction onset potentials of the polymers are versus Fc/Fc^+.

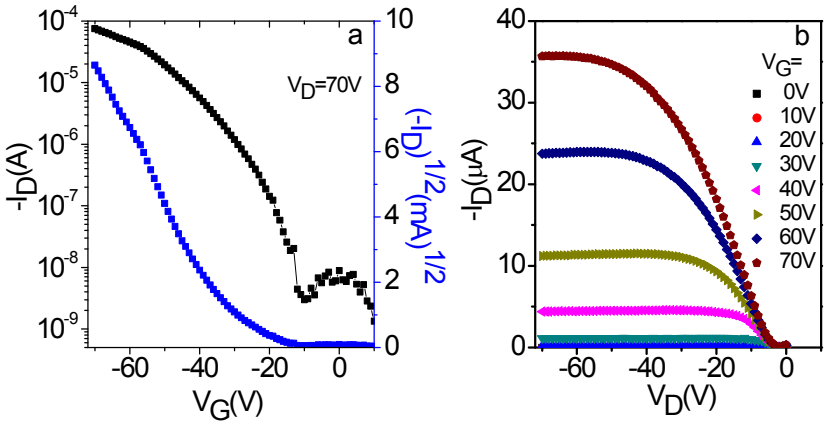

Figure S3. Output (a) and transfer (b) characteristics of OFETs based on pristine films of P(1FIID-BT).

Table S3. OFET Devices Performance of P(1FIID-BT).

$T_{postanneal}$ [°C]	μ_h [$cm^2V^{-1}s^{-1}$]	V_T [V]	$Log(I_{on}/I_{off})$
pristine	0.33	-29.8	4-5
150	0.42	-15.5	5-6
200	0.40	-6.4	5-6

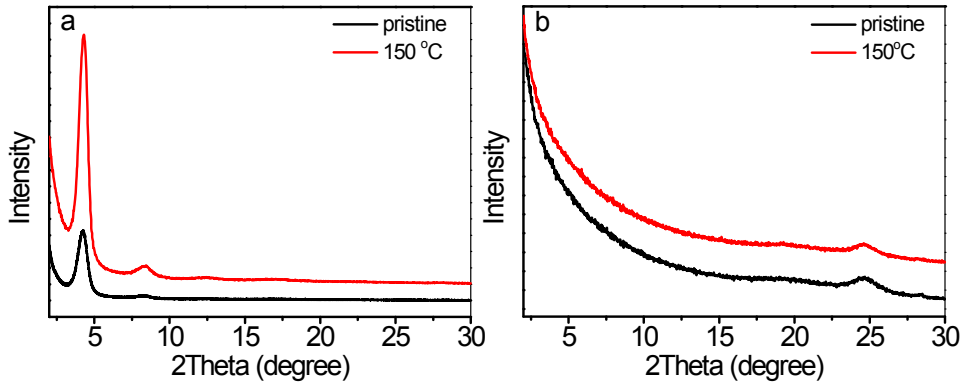

Fig. S4 Out-of-plane (a) and in-plane (b) XRD patterns of P(1FIID-BT) films before and after thermal annealing (150 °C for 20 min).

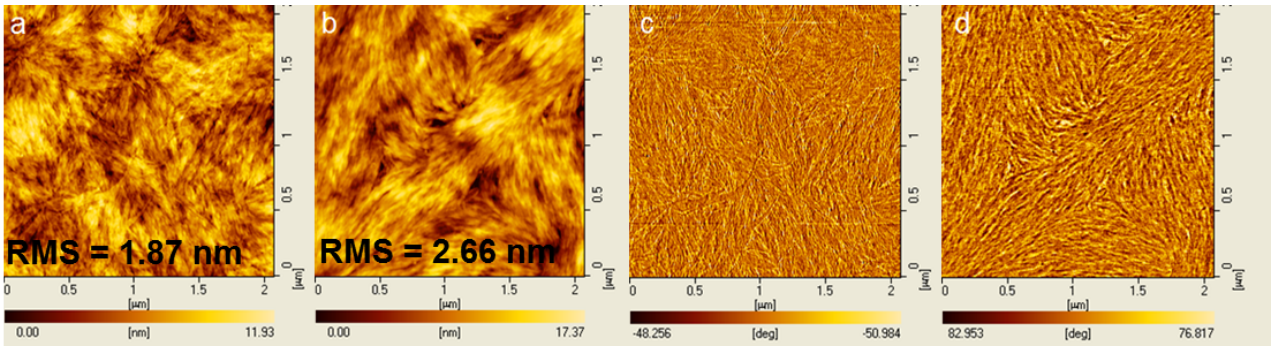

Fig. S5 AFM height (a, b) and phase images (c, d) of P(1FIID-BT) film before (a, c) and after annealing at 150 °C (b, d).

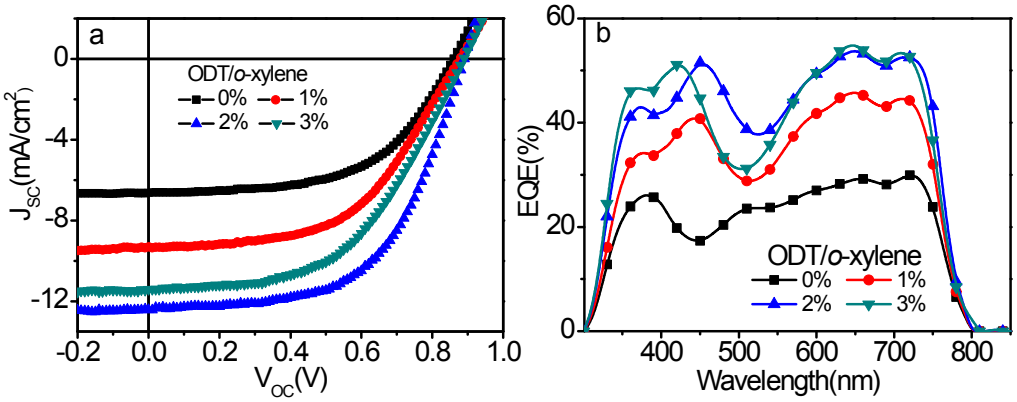

Fig. S6 J-V (a) and EQE (b) curves of PSC devices (P(1FIID-BT)/$PC_{61}BM$ = 1:1.5 (w/w)) with a different amount of ODT as additives.

Table S4. Device Performance of Conventional PSCs Based on P(1FIID-BT)/$PC_{61}BM$ (1:1.5) with Different Amount of Additives.

ODT [%]	V_{OC} [V]	J_{SC}[a] [mA cm^{-2}]	FF	PCE[b] [%]
0	0.86	6.63(6.36)	0.56	3.19(3.16)
1	0.88	9.30(9.61)	0.53	4.33(4.31)
2	0.89	12.41(11.82)	0.57	6.29(6.00)
3	0.89	11.41(11.35)	0.52	5.28(5.15)

[a)] The values in parentheses are calculated from EQE. [b)] The values in parentheses are the average of 4 devices.

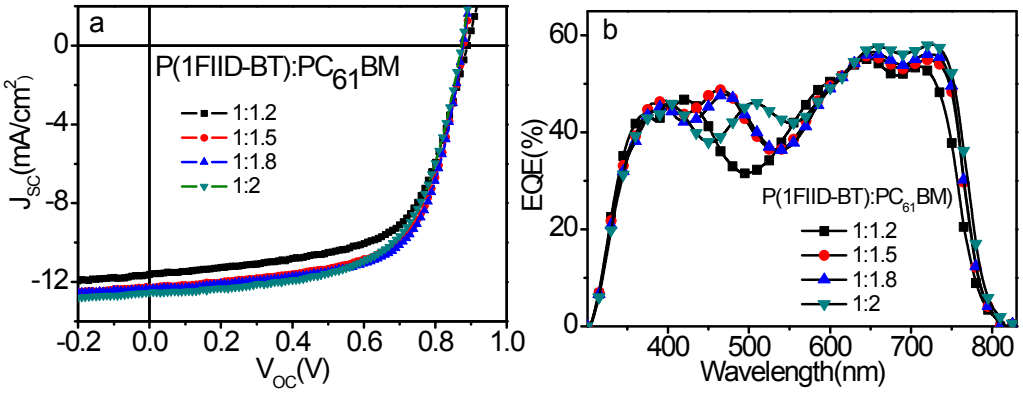

Fig. S7 *J*-V (a) and EQE (b) curves of inverted PSC devices with 2% ODT as additives.

Table S5. Device Performance of Inverted PSCs Based on P(1FIID-BT)/$PC_{61}BM$ with Different Weight Ratio.[a]

P(1FIID-BT): $PC_{61}BM$	ODT [%]	V_{OC} [V]	J_{SC}[b] [mA cm^{-2}]	FF	PCE[c] [%]
1:1.2	2	0.89	11.61(11.36)	0.62	6.40(6.27)
1:1.5		0.88	12.28(12.09)	0.64	6.92(6.81)
1:1.8		0.88	12.36(12.08)	0.65	7.07(6.91)
1:2		0.87	12.55(12.46)	0.63	6.87(6.83)

[a)] 2 V% DOT was used as additives. [b)] The values in parentheses were calculated from EQE. [c)] The values in parentheses are the average of 4 devices.

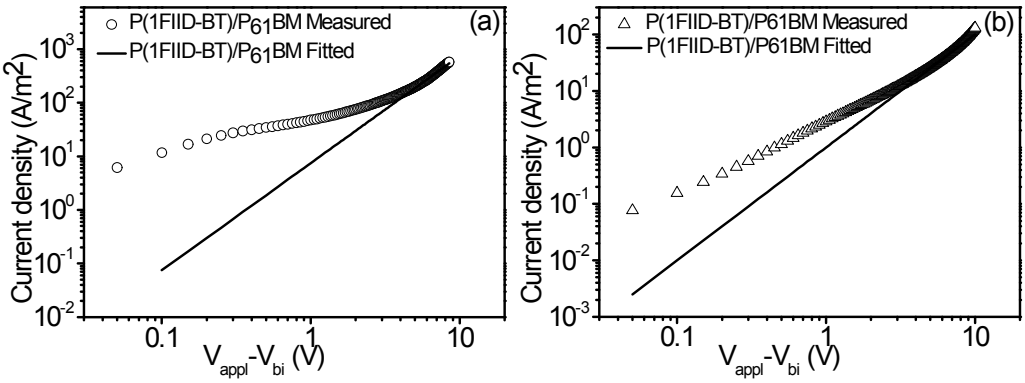

Fig. S8 *J*-V characteristics of hole-only (a) and electron-only (b) devices of P(1FIID-BT)/$PC_{61}BM$ (1:1.8, w/w). Lines represent the fitting results using a model of single-carrier space-charge-limited current with field-dependent mobility. Film thickness was ca. 300 nm.